Nanoscale

PAPER

View Article Online
View Journal | View Issue

CrossMark click for updates

Cite this: *Nanoscale*, 2017, **9**, 3150

Chemical routes to discharging graphenides†

Stephen A. Hodge,[a] David J. Buckley,[b] Hin Chun Yau,[a] Neal T. Skipper,[b] Christopher A. Howard[b] and Milo S. P. Shaffer*[a]

Received 30th December 2016,
Accepted 7th February 2017

DOI: 10.1039/c6nr10004j

rsc.li/nanoscale

Chemical and electrochemical reduction methods allow the dispersion, processing, and/or functionalization of discrete sp^2-hybridised nanocarbons, including fullerenes, nanotubes and graphenes. Electron transfer to the nanocarbon raises the Fermi energy, creating nanocarbon anions and thereby activating an array of possible covalent reactions. The Fermi level may then be partially or fully lowered by intended functionalization reactions, but in general, techniques are required to remove excess charge without inadvertent covalent reactions that potentially degrade the nanocarbon properties of interest. Here, simple and effective chemical discharging routes are demonstrated for graphenide polyelectrolytes and are expected to apply to other systems, particularly nanotubides. The discharging process is inherently linked to the reduction potentials of such chemical discharging agents and the unusual fundamental chemistry of charged nanocarbons.

Introduction

A variety of chemical and electrochemical methods of producing reduced fullerene, carbon nanotube and graphene polyelectrolyte salts, have been developed in recent years; the species are known as fullerides, nanotubides and graphenides, respectively.[1–11] These salts are attractive as they allow the nanocarbons to dissolve spontaneously in a variety of polar, aprotic solvents (such as *N*,*N*-dimethylformamide [DMF], *N*-methyl-2-pyrrolidone [NMP], dimethylacetamide [DMAc], dimethylsulfoxide [DMSO]) without the requirement for typical destructive high-shear methods (ultrasonication[12,13] or shear mixing[14]) or repetitive ultracentrifugation steps.[15] The ability to tune the charge/carbon stoichiometry also allows the purification of as-produced nanocarbon powders without the necessity for aggressive oxidative treatments.[5,16] However, in the reduced state, the nanocarbon salts are highly reactive and must be handled under inert atmosphere. The reactivity can be beneficial as it allows the individualised nanocarbons to be covalently-functionalized, using a wide range of electrophilic, radical and redox based reagents.[7,9,17–20] Compared to other functionalization strategies, such as the common use of strong acids to prepare carboxylated nanotubes[21] or graphene oxide,[22] the reductive approach is appealing, as the connectivity of the carbon framework is maintained, and damage minimised. On the other hand, even low level covalent functionalization[23] (<5 at%) intrinsically interrupts the sp^2 conjugation which is responsible for the mechanical and electronic properties of interest. In cases where charging is used only for processing, purification, sorting, or assembly, it is desirable to remove the charge without functionalization.

Polyaromatic hydrocarbon (PAH) radical anions are well studied and have been shown to react in a number of ways;[24] with atmospheric components such as water or CO_2, alkali metal naphthalenides form dihydrogenated or dicarboxylated naphthalenes, respectively.[24,25] In the absence of excess alkali metal, approximately half of the parent PAH is recovered unchanged.[25] The difunctional product is favoured due to rapid electron transfer from the naphthalenide anion to the monofunctionalised naphthalene.[26] In the presence of excess alkali metal, the parent PAH is completely converted to the difunctional derivative.[25] Whilst providing an interesting comparison, the naphthalenides can be expected to react more straightforwardly than nanocarbons, for two reasons. Firstly, the molecular reduction potential is well defined and consistently sufficient to reduce even CO_2; in contrast, graphenide species have a continuously variable reduction potential, depending on degree of (dis)charging, with a generally small absolute value. Secondly, napthalenide has C–H bonds where substitutions can occur, whereas functionalisations of graphene either depend on defect/edge sites, or a less favourable local sp^3 site formation. The competition between hydrogenation of graphite intercalation compounds (GICs) and hydrogen evolution, in protic conditions has been shown to depend on a range of factors including the size of the proton-donor,

[a]*Department of Chemistry, Imperial College London, SW7 2AZ, UK.*
E-mail: m.shaffer@imperial.ac.uk
[b]*Department of Physics and Astronomy, University College London, WC1E 6BT, UK*

† Electronic supplementary information (ESI) available: Video microscopy of KC_8 powder exposed to air and further supporting characterization (XPS, UV-vis absorption spectroscopy, NMR). See DOI: 10.1039/c6nr10004j

the effects of edges, and the choice of solvent,[27] as well as the degree of charging.[17] For almost all radical anions, exposure to atmospheric oxygen causes radical quenching and the formation of the superoxide anion, $O_2^{\bullet -}$.[28] Whilst this quenching limits the further reactivity of simple PAHs such as naphthalene, the generated superoxide species may have a destructive impact on larger, less pristine polyaromatic structures such as graphene.[29]

Typically, exposure of nanocarbon polyelectrolyte salt solutions to the atmosphere causes agglomeration of the carbon species due to rapid discharging by reaction with atmospheric components.[29] Even in cases where the charged nanocarbon is utilised as a reducing agent towards organic reagents such as alkyl halides,[11] or metal salts/complexes,[31,32] the nanocarbon may retain sufficient charge that further oxidation events occur on exposure to the ambient environment.[29] Due to the complex electronic density of states, even in these individualised species, the reactivity is dependent on the charge density on the nanocarbon framework, as well as the redox potential of the reagent.[29,31,32] The specific degree of graphene oxidation is likely to be a complex function of the degree of charging and the nature of the graphitic starting material, in terms of flake size and defect distribution, as shown for other types of deliberate graphenide fucntionalisation.[33]

In the past, a variety of *ad hoc* approaches have been used to remove unwanted charge on nanocarbons, although in fact, some of these treatments are known to induce some secondary reaction, leading to hydroxylation or hydrogenation, under certain circumstances.[29] These treatments have included the exposure of solutions or deposited thin films to different gas atmospheres[34,35] (atmospheric air, dry air, dry oxygen), solvents[17,32,36] (*e.g.* alcohols), electrochemical discharge,[5,29,35] or alkali-metal sublimation[37] (from film or powdered samples). Specifically, for GICs, acid treatment (6 M HCl) in an oxygen-free environment[38] afforded air-stable compounds with high electrical conductivity (up to 1.4×10^5 S cm^{-1}); although not assessed, this route may lead to hydrogenation route, as found in the older GIC literature.[27,39–41] Generally, solution-phase discharging results in aggregation of the graphenide species due to the minimisation of electrostatic repulsion. However, very recently, air exposed graphenide was successfully re-dispersed in degassed water explained by the spontaneous adsorption of OH^- ions on the graphene surface following oxidation.[42] Gas species are able to displace surface OH^- ions, hence degassing is proposed to provide an energy barrier to reaggregation.

Understanding the effect of the discharge process is generally complicated by sample heterogeneity and a variety of other simultaneous changes, such as covalent modification,[34] selective/competitive reactions,[27,41] and fractionation/purification.[5,16] Discharging with gases is simple, but difficult to monitor quantitatively. Sublimation treatments require rigorous set ups and may not go to completion. In this report, a variety of chemical discharging agents are compared, allowing a definitive control of stoichiometry, and the opportunity to explore redox potential dependence. One recent approach utilised benzonitrile solvent which reacts with graphenide to produce the red coloured benzonitrile radical anion.[43] Benzonitrile has a reduction potential of −2.74 V *vs.* Ag in DMF,[43] is a known redox catalyst[44] and without careful processing, reversible electron transfer back to the graphene might be expected.

For the fundamental study presented here, graphenide solutions were selected as a representative nanocarbon, as they have a simpler electronic density of states than nanotubes, and avoid metal catalyst contaminants. For cleanliness, graphenide solutions were produced from the vapour-intercalated graphite intercalation compound (GIC), KC_8, which is dispersed as discretely-charged monolayer sheets in polar aprotic solvents.[4,35] These graphenide solutions were then chemically discharged and washed to remove by-products. For practical application, the chemical discharging agent should be added in excess relative to nanocarbon charge, undergo pure electron transfer without any covalent bond formation with the nanocarbon, and be easily removed.

In previous studies,[31] the reactivity of reduced nanocarbons has been related to the reduction potential given by the shift in Fermi level with respect to the nanocarbon electronic density of states (Fig. 1). At high charge densities, corrections

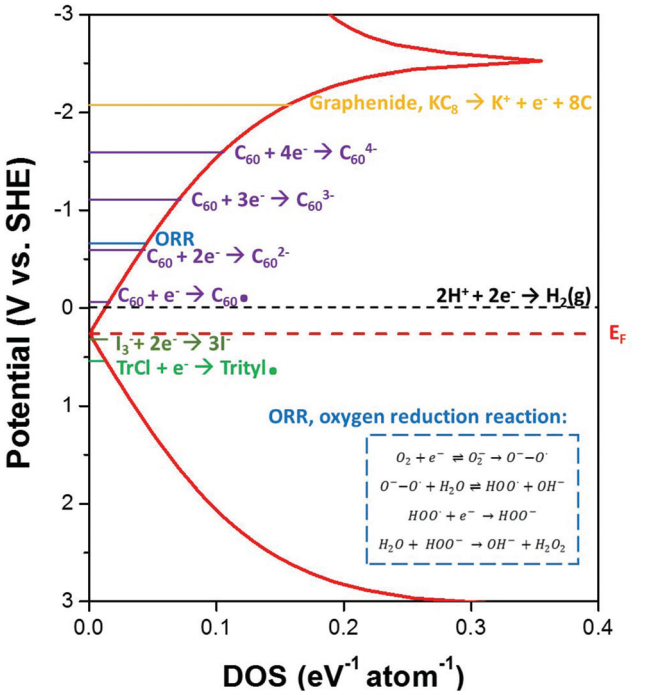

Fig. 1 Schematic graphene density of states (tight binding approximation) showing the measured reduction potential for graphenide species relative to the reduction potentials of the discharging agents used in this study. Discharging with all these reagents is hypothesised to discharge the graphene to a level lower than the oxygen reduction potential, to avoid any unwanted functionalizations upon exposure of samples to ambient conditions. The oxygen reduction potential[30] in polar aprotic solvent, *N*,*N*-dimethylformamide (DMF), at a graphite powder electrode is highlighted by the blue line. Inset shows the mechanism for oxygen reduction to the superoxide radical anion, and decomposition of the superoxide in the presence of water to form peroxide; which have been proposed to functionalize nanocarbons.[29]

for Coulombic effects may be taken into account *via* quantum capacitance.[31] KC_8 has a reduction potential as high as −2.04 V *vs.* standard hydrogen electrode, SHE.[31] The simplest route to chemical discharging is, therefore, to utilise redox or electron transfer reactions where potential side-products remain unreactive towards the nanocarbon. An alternative viewpoint considers nanotubide and graphenide functionalizations to be governed by radical-based mechanisms,[7] thus, an approach that generates an explicit, stable, radical species which is sacrificially destroyed upon exposure to the atmosphere could be utilised. Based on the experimentally determined reduction potential of pristine graphene (+0.263 V *vs.* SHE),[35] three possible reagents were proposed as ideal candidates for quenching: 1. iodine; 2. fullerene; 3. triphenylmethyl chloride, before exposure to the atmosphere.

The discharging of charged nanocarbons upon exposure to oxygen has been proposed to be governed by the oxygen reduction reaction (ORR).[29] The ORR in aqueous solutions occurs mainly by two pathways: the direct 4-electron reduction pathway from O_2 to H_2O, and the 2-electron reduction pathway from O_2 to hydrogen peroxide (H_2O_2). In non-aqueous aprotic solvents[30,45] such as that used here (NMP), the 1-electron reduction pathway from O_2 to the superoxide radical anion ($O_2^{\bullet-}$) can occur with subsequent formation of peroxide upon reaction with water (see Fig. 1 inset). The reduction of $O_2/O_2^{\bullet-}$ in DMF has been observed to occur at a graphite powder electrode at −0.646 V *vs.* SHE.[30] Hof *et al.*[29] used this reaction mechanism to explain the resulting hydroxylation and protonation of intermediately activated carbon nanotubides.

The pathways to chemical discharging using the proposed reagents are shown in Scheme 1. Iodine, I_2, is a widely-used reagent and in solution, iodine will bind with iodide (I^-) to form triiodide (I_3^-) in equilibrium. This redox couple is commonly used in dye-sensitized solar cells and has a potential of +0.29 V *vs.* SHE in acetonitrile, close to that of the neutral nanocarbon species.[46] Subsequent reduction to I^- is hypothesised to combine with the alkali-metal counterions to generate the metal iodide salt (KI). These salts can then be washed away due to their high solubility in water. Iodine discharging can be carried out in solution-phase due to its high solubility in many solvents, or in the vapour-phase due to its slight degree of sublimation at room temperature[47] (vapour pressure = 0.031 kPa). In fact, the use of iodine has been demonstrated in the oxidation of fullerenide anions for the extraction of fullerenes from solution.[48]

Fullerene, C_{60}, is a well-known nanocarbon that, unlike carbon nanotubes and graphene, has distinct molecular orbitals for discrete electron transfer leading to the formation of fulleride anions,[49] C_{60}^{n-} where n = 1–6. The reduction potentials for the fulleride anions in DMF[49] are −0.13 V ($C_{60}^{0/1-}$), −0.59 ($C_{60}^{1-/2-}$), −1.18 ($C_{60}^{2-/3-}$), −1.72 ($C_{60}^{3-/4-}$) *vs.* SHE, indicating that when present in excess to potassium, such species should sufficiently discharge the graphenide. Fulleride anions also vary in colour, dependent on the number of electrons transferred, thus, charge transfer has a visual endpoint.

Fulleride reactions are well studied;[50] upon exposure to the atmosphere, fulleride anions will react with oxygen to form superoxide, or can be protonated by water. However, the aerobic oxidation of singly-charged fullerides can be fairly slow, and as a result, some C_{60}^- solids are air stable.[50]

Triphenylmethyl chloride, TrCl, is a very well-studied compound, readily forming the highly stable Gomberg trityl radical[51] that can be observed *via* its characteristic yellow colour. An equilibrium exists between the yellow-coloured radical and a quinoid dimer, since the molecule is unable to form the hexamethylethane dimer due to steric effects.[52] These same steric effects are likely to hinder grafting to the nanocarbon structure. In acetonitrile, the reduction potential of TrCl is approximately +0.51–0.53 V *vs.* SHE.[53,54] TrCl has been reacted in the past with lithium naphthalenide to generate the parent naphthalene and trityl radical dimer.[55]

The focus of this paper is to distinguish if and which chemical discharging agents can provide a simple and effective way to avoid oxidations and adventitious functionalizations in restoring pristine nanocarbons. Covalent functionalizations, by-products and other structural effects are monitored by a combination of techniques including thermogravimetric analysis (TGA), X-ray photoelectron spectroscopy (XPS) and Raman spectroscopy, combined with chemically-specific tagging reactions.

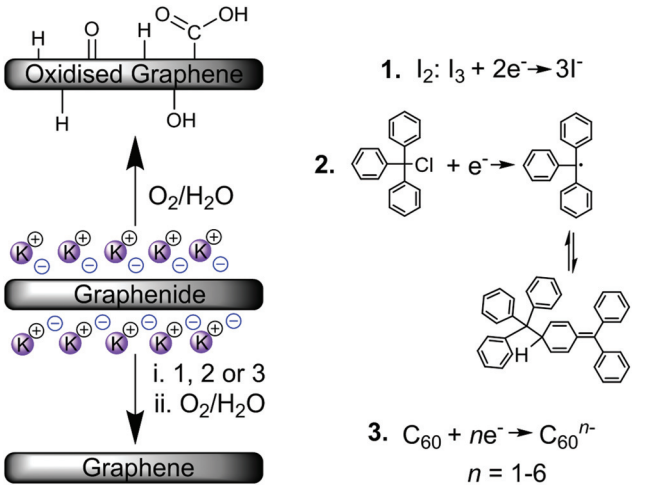

Scheme 1 Discharging of graphenide polyelectrolytes under ambient conditions (oxygen/water[29]) and the chemical discharging agents investigated (1. iodine, I_2, 2. triphenylmethyl chloride, and 3. fullerene, C_{60}).

Experimental

Materials and methods

Preparation of graphenide dispersion. Natural flake graphite was purchased from Graphit Kropfmühl GmbH (RFL grade, 99.9% purity, min. 90% >160 μm). KC_8 was prepared by the vapour transport method[56] generating the characteristic gold coloured stage 1 GIC. For each experiment, 30 mL, NMP (anhydrous grade, 99.5%, further dried by 4 Å molecular sieves,

both purchased from Sigma-Aldrich, UK), was added to 10 mg KC_8 in a 100 mL Young's tap Schlenk tube inside a MBraun LabmasterSP glove box with levels of H_2O and O_2 below 1 ppm at all times. The sample tube was removed from the glove box, mildly sonicated for 30 min (ultrasonic cleaner, VWR, UK) and returned to the glove box for discharging reactions.

Chemical discharging reactions. Iodine (anhydrous beads, −10 mesh, 99.999%) and trityl chloride (97%) were purchased from Sigma-Aldrich. C_{60} powder (99.5%) was obtained from SES Research, Houston, US. Chemical discharging reagents were added in a three times excess relative to potassium. In the case of iodine discharging, a stock solution of iodine in NMP (11.3 g L^{-1}) was prepared in advance to ensure that the sublimation of iodine pellets did not contaminate the glove box atmosphere.

KC_8 vacuum annealing. The KC_8 powder was put into a stainless steel KF25 tube (0.5 m length) and baked at 700 °C, 10^{-6} mbar for 24 h. For the 1000 °C anneal, the 700 °C annealed KC_8 was exposed to air for ~5 seconds for loading into a sealed graphite crucible inside a graphite furnace. The crucible was baked at 1000 °C at 10^{-6} mbar for 24 h. All temperature ramps were controlled to 5 °C min^{-1}.

Characterisation methods

X-ray photoelectron spectroscopy (XPS). XPS spectra were recorded using a Thermo Scientific K-Alpha instrument using focused (400 μm spot) monochromatic Al-Kα radiation at a pass energy of 40 eV. The binding energies were referenced to the sp^2 C 1s peak of graphite at 284 eV.

Thermogravimetric analysis-mass spectrometry (TGA-MS). TGA-MS was performed using a Mettler Toledo TGA/DSC 1 with a GC200 flow controller. The TGA was coupled to a mass spectrometer (Hiden MS fitted with a 200 a.u. quadrupole sensor). Samples were heated from 30 to 100 °C at 35 °C min^{-1}, and then held isothermally at 100 °C for 30 min in an inert atmosphere (N_2, 60 mL min^{-1}) to remove residual moisture. The temperature was then ramped to 800 °C at 10 °C min^{-1}. Oxidative TGA of as-received natural flake graphite and vacuum annealed KC_8 at 700 °C and 1000 °C were performed in air (60 mL min^{-1}) with a temperature ramp from 100–1100 °C.

Raman spectroscopy. Raman spectroscopy was performed using a Renishaw InVia micro-Raman Spectrometer using a 532 nm laser using <1 mW laser power and 1800 gr mm^{-1} grating. At least 30 spectra were measured for each sample over the range 1250–3250 cm^{-1}.

UV-vis absorption spectroscopy. UV-vis spectroscopy was performed using a Perkin Elmer Lambda 950 spectrophotometer Samples were dissolved in toluene and spectra were recorded from 200 to 800 nm with a resolution of 1 nm, using a 10 mm path length UV quartz cuvette.

Nuclear magnetic resonance (NMR) spectroscopy. NMR spectra were acquired using a Bruker AM 400 spectrometer operating at 9.4 T. Samples were dissolved in $CDCl_3$ and all spectra (for ^1H and ^{13}C) were recorded with 16 scans and D1 = 1 s. Distortionless enhancement polarisation transfer (135 DEPT) NMR spectra was acquired with 386 scans with D1 = 1 s. All chemical shifts (δ) are given in ppm, where the residual $CHCl_3$ peak was used as an internal reference for ^1H NMR (δH = 7.28 ppm), and for ^{13}C NMR (δC = 78.23 ppm).

Scanning electron microscopy-energy dispersive X-ray (SEM-EDX) spectroscopy. SEM-EDX was performed using a high resolution field emission gun scanning electron microscope (FEGSEM) Leo Gemini 1525, with a built-in energy dispersive and wavelength dispersive X-ray spectrometer (EDX) (INCA, using INCA suite software V4.15, 2009, Oxford Instruments Plc., UK). Graphitic samples for SEM/EDX spectroscopy were contacted to aluminium stubs using silver dag (all SEM preparation products purchased from Agar Scientific, UK).

Results and discussion

Graphenide exposure to ambient air

To confirm the product of the hypothesised oxygen reduction reaction (ORR), KC_8 dispersions were discharged by exposure to ambient air. Exposure of graphenide/NMP solution to the atmosphere resulted in the slow precipitation of graphene (over 72 hours) presumed to be sufficient to reach complete discharge. The resulting material was filtered through a 100 nm pore size PTFE membrane and washed with NMP, water, chloroform and ethanol (100 mL of each) to remove the potassium (hydr)oxide salts.

The starting graphite material had only a low oxygen content (C/O ~30; shown in Fig. 4), which increased significantly for air discharged KC_8 (C/O ~9). This ratio in the product is consistent with mildly oxidised graphene oxide (GO) or reduced graphene oxide (RGO).[57] High-resolution XPS (ESI Fig. S1†) revealed a broad O 1s signal that was fitted with two components (532.1 eV and 531.2 eV) with an approximate 60 : 40 peak area ratio that suggests the presence of both C═O and C–O bonds, respectively. Also, XPS revealed the presence of ~2–6 at% potassium remaining even after washing. This potassium could be associated with the formation of potassium carboxylates, residual KOH, or trapped potassium between graphene layers. The observation of absorbed and intercalated potassium hydroxides/alkoxides upon reaction of GICs with water or alcohols was previously reported, even following hot aqueous/acid and ethanol washing steps.[27] The discharging of a piece of KC_8 powder in air was also monitored under a microscope (ESI Movie 1†) showing rapid formation of these potassium (hydr)oxide salts on the surface of the deintercalating graphite powder.

As reported previously, the quantification of specific oxygen-containing moieties directly by XPS is challenging due to the prevalence of oxygen-related contamination and the difficulty of reliably fitting low concentration peaks in the carbon shake-up tail. An interesting improvement can be obtained by tagging each functional group with three fluorine atoms using chemically-selective reagents. Thus, for more detailed quantification, derivitization reactions of the

hydroxyl, carboxyl and carbonyl groups were performed using trifluoroacetic anhydride (TFAA), trifluoroethanol (TFE) and trifluoroethylhydrazine (TFH), respectively (Fig. 2a), using a methodology described by Buono *et al.*[58]

TFAA reacts selectively with hydroxyl groups with a 1 : 1 stoichiometry and high selectivity. In this case, a strong F 1s peak appeared at 688.2 eV corresponding to 12.3 at%, while the O 1s peak downshifted, gaining a prominent shoulder. The fluoroacetate moiety bears both a carbonyl and methoxy functionality, that give rise to the two fitted peaks at 531.7 eV and 529.6 eV, respectively.

Carboxyl groups were quantified by reaction with TFE, again with a 1 : 1 stoichiometry. While the F 1s signal is observed at 688.4 eV, there is only a low fluorine content in the TFE treated material (2.2 at%). Carbonyl groups were quantified by TFH, with the appearance of both F 1s and N 1s signals at 688.2 eV and 400.3 eV, respectively. These signals corresponded to 15.3 at% and 6.9 at%, respectively. The concentrations of specific oxygen moieties were quantified using expressions outlined by Wepasnick *et al.*[59] using the C, N and F atomic concentrations. The concentrations of oxygen present as carboxyl, carbonyl and hydroxyl groups equate to 1.4, 6.5 and 4.6 at%, respectively. While this total oxygen content is slightly higher than that expected from the original untagged XPS (~10 at%), there is clear indication that hydroxyl and carbonyl (ketone) groups comprise the majority of functionalities present on the air discharged graphenide material. Except for the TFH case, in which nitrogen is explicitly grafted, the N signals are small (<0.6 at%), indicating that radically-initiated grafting reactions involving the NMP are not a significant factor.

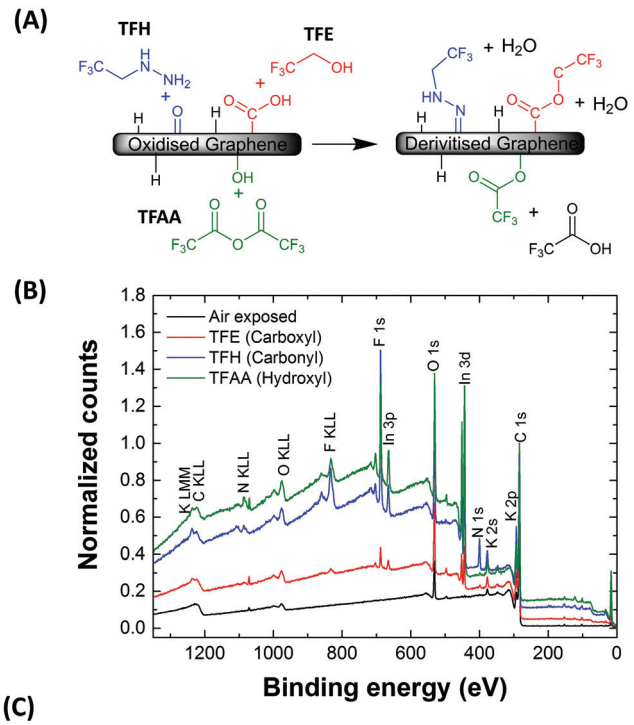

(C)

Air exposed KC_8		TFE (Carboxyl)		TFH (Carbonyl)		TFAA (Hydroxyl)	
Peak	At %	Peak	At %	Peak	At %	Peak	At %
C 1s	88.84	C 1s	78.68	C 1s	56.99	C 1s	63.22
O 1s	8.90	O 1s	15.02	O 1s	14.80	O 1s	20.83
K 2p	2.26	K 2p	4.08	K 2p	6.01	K 2p	3.64
		F 1s	2.21	F 1s	15.28	F 1s	12.31
				N 1s	6.92		

Fig. 2 (A) Scheme showing derivitization reactions for the XPS quantification of air discharged graphenide (KC_8), using TFAA (hydroxyl groups), TFE (carboxyl groups) and TFH (carbonyl groups). (B) Survey XPS spectra following air discharging of KC_8 and following the derivitisation reactions. Indium signals arise due to the indium foil substrates used. (C) Table showing elemental analysis of each sample based on the areas of the regions fitted in the hi-resolution spectra in Fig. S1.†

Chemical discharging reactions

Chemical discharging reagents were added in a three times excess relative to potassium. The addition of 5 mL iodine/NMP stock solution (see Methods section in ESI†) to the graphenide/NMP solution resulted in the rapid flocculation of graphene. The sample was removed from the glove box, filtered and washed as above to remove excess iodine and potassium iodide.

For the case of fullerene discharging, due to its insolubility in NMP, C_{60} powder was added directly to the graphenide/NMP solution. A dark red solution was observed within 30 minutes, whilst the graphene agglomerated. The dark red solution was confirmed by UV-vis absorption spectroscopy to be the fulleride radical anion, $C_{60}^{\bullet -}$ (ESI Fig. S2†). The highly soluble fulleride anions were simply washed away with vacuum filtration to leave behind the discharged graphene powder. Following prolonged exposure to the ambient atmosphere, the initial dark red filtrate turned yellow/brown, indicating sacrificial reaction of the fulleride anion with oxygen, similar to fulleride anion reactivity described by Reed.[50] Removing excess uncharged fullerene was more challenging due to its strong adsorption to graphene surfaces *via* van der Waals interactions.[60] Several washing steps with toluene and CS_2 were, therefore, required, monitoring the filtrate with optical absorption spectroscopy.

The addition of triphenylmethyl chloride, TrCl, to graphenide/NMP solutions resulted in the formation of a yellow solution, indicative of trityl radical formation. The immediate precipitation of the graphenide was observed. The expected formation of trityl peroxide upon exposure of the trityl radial to the atmosphere was not observed. Instead, following workup with NMP/ethanol, the filtrate colour slowly changed to red. The red solution was subsequently dried using a flow of nitrogen gas (7 days) followed by vacuum drying of the residual material (2 days). Thin-layer chromatography of the remaining red solid revealed two compounds; further characterisation using by UV-vis, ^{1}H and ^{13}C NMR confirmed the presence of unreacted trityl chloride, and the side-product trityl ethyl ether (ESI Fig. S3 and S4†) as a result of the ethanol washing step. No evidence of reaction with NMP was found.

Following chemical discharging and exposure of samples to ambient conditions, samples were characterised using a com-

bination of thermogravimetric analysis-mass spectroscopy (TGA-MS), X-ray photoelectron spectroscopy (XPS) and Raman spectroscopy to probe the effectiveness in avoiding covalent functionalization of the nanocarbon surfaces.

TGA–MS (Fig. 3a) was performed in an inert atmosphere (N_2, 60 mL min^{-1}). The origin of the small (~1 wt%) increase at high temperatures is unknown but has been observed previously in other studies of graphene in inert atmospheres.[61,62] All solution-processed graphenides contain residual NMP solvent, trapped upon discharging and reagglomeration; even with extended washing, up to ~1–2 wt% NMP remains. Air-discharged graphenide samples showed a significant weight loss (2.15 wt%) at ~400 °C corresponding to m/z 44 (CO_2), consistent with the carboxyl content estimated from XPS. Both I_2 and TrCl discharged KC_8 had a similar decomposition feature at ~400 °C, although only at a much lower level, around 0.3 wt% in both cases. The higher degree of functionalisation implied by XPS may reflect the technique's surface sensitivity and a greater concentration of oxygen groups forming on the surface of partially exfoliated or restacked graphenide. More importantly, however, TGA/MS showed no evidence for grafting of phenyl or iodide containing groups following TrCl and I_2 discharging, respectively. C_{60} discharged graphenide, showed no weight loss, other than solvent, indicating the recovery of a highly pristine structure, and successful removal of all unreacted fullerenes.

The chemical discharging agents were also compared against traditional high temperature, ultra-high vacuum treatments that are used to directly sublime the alkali-metal from the KC_8 crystal.[37] Samples were annealed at 700 °C and 1000 °C at 10^{-8} mbar. Oxidative TGA (Fig. 3b) revealed that 700 °C treatment is sufficient to remove the alkali metal, while further heating to 1000 °C allows for the removal of other silicon and aluminium oxide impurities that are typically found in naturally mined graphite,[63] determined by SEM-EDX (Fig. 3b inset). While this approach is effective at removing the alkali metal, the equipment costs and process times are not suited to large-scale processing. Additionally, the graphite restacks and loses any intended covalently-bound functional groups.

XPS spectra (Fig. 4) confirm that near pristine carbon surfaces were recovered for all chemically discharged graphene polyelectrolytes, which showed an oxygen content (C/O ~20–50), similar to the starting material (C/O ~30), and significantly lower than the air-quenched sample discussed above (C/O ~9). The effectiveness of potassium removal was derived from high-resolution XPS of the C 1s and K 2p regions, identifying KC_x where x is 40, 132, 174 and 203 for air, I_2, C_{60} and TrCl discharged graphenides, respectively. The chemical discharging reactions remove a significantly larger fraction of the potassium than the standard air exposure and wash which leaves oxygen-containing groups that can associate with the potassium ions. Since, XPS is a highly surface sensitive tech-

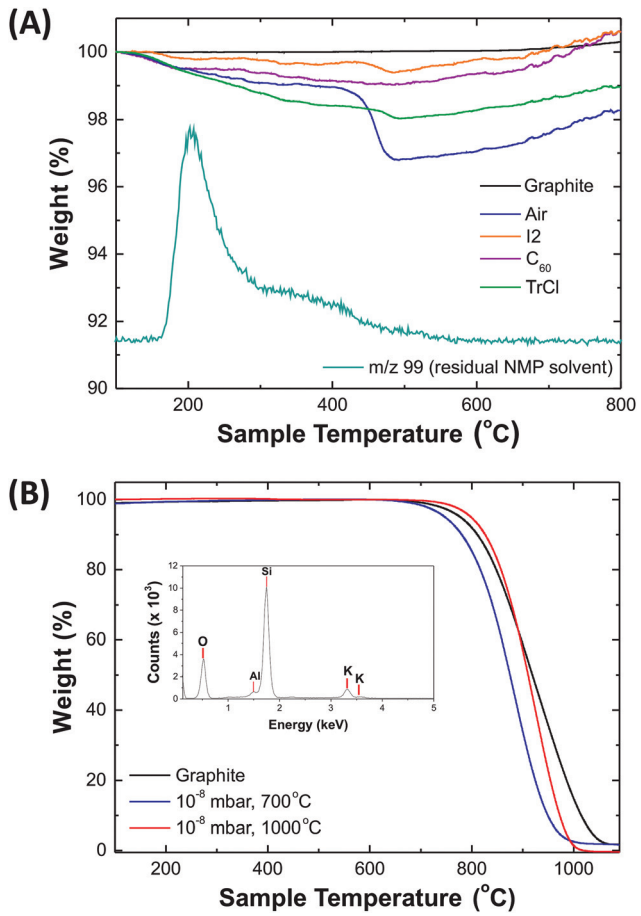

Fig. 3 (A) TGA of as-received natural flake graphite and discharged KC_8 materials in a nitrogen atmosphere. The dark cyan curve represents the mass spectrum of the fragment m/z 99 corresponding to the NMP solvent that causes the weight loss between 200–400 °C. This m/z trace if for the C_{60} discharged material; the other samples showed a similar trace though with lower signal to noise. (B) Oxidative TGA of as-received natural flake graphite and vacuum annealed KC_8 at 700 °C and 1000 °C. Inset shows the energy dispersive X-ray (EDX) spectra of sublimed silica, alumina and potassium following vacuum annealing at 1000 °C.

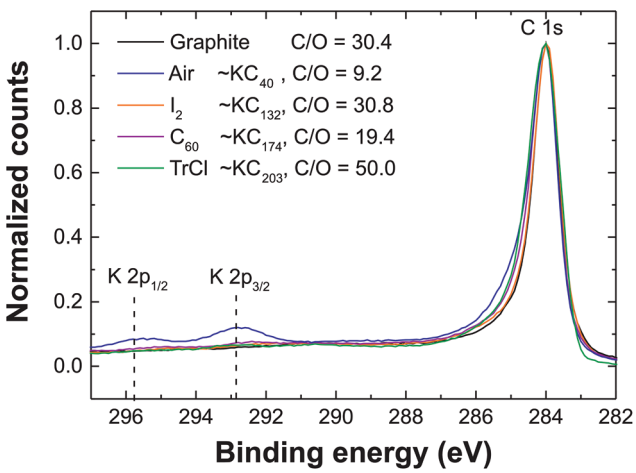

Fig. 4 XPS of the C 1s region following the discharging of graphenide (KC_8) with air and chemical reagents.

nique, further corroboration was provided by Raman spectroscopy, below. In the case of I_2 discharging, very small iodine signals (<0.02 at%) were observed at 631.6 eV and 620.3 eV assigned to the metal iodide (KI); similarly, TrCl discharged graphenide revealed a small chlorine peak at 199 eV (~0.3 at%) consistent with the presence of residual metal chloride (KCl).[64]

The Raman spectra of the starting graphite powder and various treated materials measured at 532 nm, confirm the importance of the discharging process (Fig. 5a) and are consistent with the XPS data. The intensity ratio between the D and G peaks, $I(D)/I(G)$, gives an indication of structural disorder (Fig. 5b).[65] Most significantly, the $I(D)/I(G)$ ratio shows that the initial natural graphite powder becomes more defective after air quenching; annealing to 1000 °C is required to regain a spectrum similar to the pristine state. The statistical error associated with the I_2 experiments is relatively large, but discharging with both C_{60} and TrCl clearly restored the $I(D)/I(G)$ to the original level. The original and restacked (thermally annealed) graphites show only weak D′ peaks and characteristic double featured 2D peaks. The chemically discharged species show stronger, sharper D′ peaks, and less asymmetric 2D peaks, consistent with retaining a higher degree of exfoliation.[66]

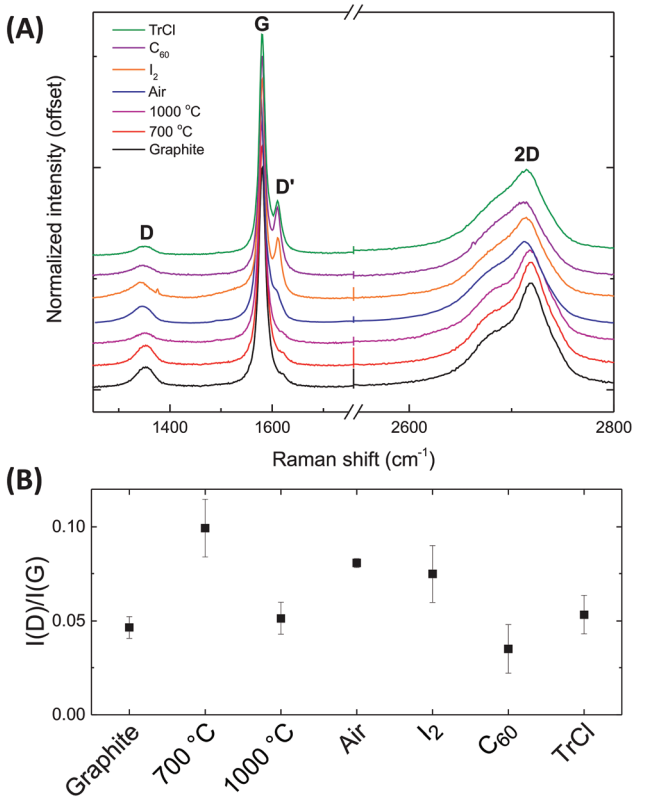

Fig. 5 (A) Raman spectra of as-received graphite, thermally annealed and chemically discharged graphenides. Raman spectra showing the D, G, D′ and 2D peak regions. Spectral intensity is normalized to the G peak in each case and offset for clarity. (B) Intensity ratio plots of $I(D)/I(G)$ for the samples described in (A). Error bars indicate the standard error.

Conclusions

Discharging graphenides by exposure to ambient conditions has been demonstrated to lead to a degree of oxidation likely dependent on the intrinsic graphite structural quality. This oxidation is mechanistically described by the oxygen reduction reaction in aprotic media. Effective solution phase discharging of graphenide species has been demonstrated using three different chemical agents. Iodine, fullerene and triphenylmethyl chloride showed minimal evidence of any surface functionalization following exposure of the discharged solutions to air based on complementary TGA, XPS and Raman spectroscopy. The discharging mechanisms were found to be linked to the appropriate electrochemical reduction potentials of the discharging agents; however, kinetic limitations leave some small fraction of intercalated alkali metal within the structure (~0.5–0.75% of the potassium introduced initially). While TrCl discharging showed best results, the possibility of using iodine as a vapour phase quenching agent for deposited nanocarbon films may be attractive for device manufacture. Alternatively, these discharging agents could be used in the wet spinning of graphene and carbon nanotube fibres. A recent study spinning such fibres from nanotubide/graphenide solutions suggested that the mechanical and electrical properties were limited by the hydrogenation of the graphene sheets in the coagulation bath.[67] It is likely that many other chemical discharging agents exist and may open up other avenues for nanocarbon processing. As well as its importance for the development of this important class of materials, this work raises interesting fundamental questions about the reactivity of discrete nanoscale species, compared to conventional molecular analogues (in this case, polyaromatic hydrocarbons), which should stimulate further experimental and theoretical studies. These chemical discharging routes, and the associated underpinning understanding, will provide a useful tool for many other doped systems, including carbon nanotubides and transition metal dichalcogenides[68] to regenerate pristine materials or avoid unwanted successive oxidations or covalent functionalization.

Acknowledgements

The authors would like to acknowledge funding from EPSRC EP/K016792/1, EP/L001896/1 and EP/K01658X/1.

Notes and references

1 C. A. Howard, H. Thompson, J. C. Wasse and N. T. Skipper, *J. Am. Chem. Soc.*, 2004, **126**, 13228–13229.
2 A. Pénicaud, P. Poulin, A. Derré, E. Anglaret and P. Petit, *J. Am. Chem. Soc.*, 2005, **127**, 8–9.
3 S. Fogden, C. A. Howard, R. K. Heenan, N. T. Skipper and M. S. P. Shaffer, *ACS Nano*, 2012, **6**, 54–62.

4 E. M. Milner, N. T. Skipper, C. A. Howard, M. S. P. Shaffer, D. J. Buckley, K. A. Rahnejat, P. L. Cullen, R. K. Heenan, P. Lindner and R. Schweins, *J. Am. Chem. Soc.*, 2012, **134**, 8302–8305.
5 S. A. Hodge, S. Fogden, C. A. Howard, N. T. Skipper and M. S. P. Shaffer, *ACS Nano*, 2013, **7**, 1769–1778.
6 S. A. Hodge, M. K. Bayazit, H. H. Tay and M. S. P. Shaffer, *Nat. Commun.*, 2013, **4**, 1989.
7 S. A. Hodge, M. K. Bayazit, K. S. Coleman and M. S. P. Shaffer, *Chem. Soc. Rev.*, 2012, **41**, 4409.
8 A. Pénicaud and C. Drummond, *Acc. Chem. Res.*, 2013, **46**, 129–137.
9 C. Jiang, A. Saha and A. A. Martí, *Nanoscale*, 2015, **7**, 15037–15045.
10 C. Jiang, A. Saha, C. Xiang, C. C. Young, J. M. Tour, M. Pasquali and A. A. Martí, *ACS Nano*, 2013, **7**, 4503–4510.
11 K. Huang, G. Delport, L. Orcin-Chaix, C. Drummond, J.-S. Lauret and A. Penicaud, *Nanoscale*, 2016, **8**, 8810–8818.
12 Y. Hernandez, V. Nicolosi, M. Lotya, F. M. Blighe, Z. Sun, S. De, I. T. McGovern, B. Holland, M. Byrne, Y. K. Gun'Ko, J. J. Boland, P. Niraj, G. Duesberg, S. Krishnamurthy, R. Goodhue, J. Hutchison, V. Scardaci, A. C. Ferrari and J. N. Coleman, *Nat. Nanotechnol.*, 2008, **3**, 563–568.
13 H. C. Yau, M. K. Bayazit, J. H. G. Steinke and M. S. P. Shaffer, *Chem. Commun.*, 2015, **51**, 16621–16624.
14 K. R. Paton, E. Varrla, C. Backes, R. J. Smith, U. Khan, A. O'Neill, C. Boland, M. Lotya, O. M. Istrate, P. King, T. Higgins, S. Barwich, P. May, P. Puczkarski, I. Ahmed, M. Moebius, H. Pettersson, E. Long, J. Coelho, S. E. O'Brien, E. K. McGuire, B. M. Sanchez, G. S. Duesberg, N. McEvoy, T. J. Pennycook, C. Downing, A. Crossley, V. Nicolosi and J. N. Coleman, *Nat. Mater.*, 2014, **13**, 624–630.
15 U. Khan, A. O'Neill, H. Porwal, P. May, K. Nawaz and J. N. Coleman, *Carbon*, 2012, **50**, 470–475.
16 A. J. Clancy, J. Melbourne and M. S. P. Shaffer, *J. Mater. Chem. A*, 2015, **3**, 16708–16715.
17 R. A. Schäfer, D. Dasler, U. Mundloch, F. Hauke and A. Hirsch, *J. Am. Chem. Soc.*, 2016, **138**, 1647–1652.
18 J. Chattopadhyay, A. K. Sadana, F. Liang, J. M. Beach, Y. Xiao, R. H. Hauge and W. E. Billups, *Org. Lett.*, 2005, **7**, 4067–4069.
19 S. Chakraborty, J. Chattopadhyay, W. Guo and W. E. Billups, *Angew. Chem., Int. Ed.*, 2007, **119**, 4570–4572.
20 F. Liang, A. K. Sadana, A. Peera, J. Chattopadhyay, Z. Gu, R. H. Hauge and W. E. Billups, *Nano Lett.*, 2004, **4**, 1257–1260.
21 M. S. P. Shaffer, X. Fan and A. H. Windle, *Carbon*, 1998, **36**, 1603–1612.
22 W. S. Hummers and R. E. Offeman, *J. Am. Chem. Soc.*, 1958, **80**, 1339–1339.
23 A. J. Marsden, P. Brommer, J. J. Mudd, M. A. Dyson, R. Cook, M. Asensio, J. Avila, A. Levy, J. Sloan, D. Quigley, G. R. Bell and N. R. Wilson, *Nano Res.*, 2015, **8**, 2620–2635.
24 N. L. Holy, *Chem. Rev.*, 1974, **74**, 243–277.
25 D. E. Paul, D. Lipkin and S. I. Weissman, *J. Am. Chem. Soc.*, 1956, **78**, 116–120.
26 R. L. Ward and S. I. Weissman, *J. Am. Chem. Soc.*, 1954, **76**, 3612–3612.
27 D. E. Bergbreiter and J. M. Killough, *J. Am. Chem. Soc.*, 1978, **100**, 2126–2134.
28 S. P. McManus and C. U. Pittman, *Organic Reactive Intermediates*, Elsevier, 1973.
29 F. Hof, S. Bosch, S. Eigler, F. Hauke and A. Hirsch, *J. Am. Chem. Soc.*, 2013, **135**, 18385–18395.
30 Y. Wei, X. Ji, X. Dang and S. Hu, *Bioelectrochemistry*, 2003, **61**, 51–56.
31 S. A. Hodge, H. H. Tay, D. B. Anthony, R. Menzel, D. J. Buckley, P. L. Cullen, N. T. Skipper, C. A. Howard and M. S. P. Shaffer, *Faraday Discuss.*, 2014, **172**, 1379–1382.
32 M. K. Bayazit, S. A. Hodge, A. J. Clancy, R. Menzel, S. Chen and M. S. P. Shaffer, *Chem. Commun.*, 2016, **52**, 1934–1937.
33 K. C. Knirsch, J. M. Englert, C. Dotzer, F. Hauke and A. Hirsch, *Chem. Commun.*, 2013, **49**, 10811–10813.
34 Z. Syrgiannis, B. Gebhardt, C. Dotzer, F. Hauke, R. Graupner and A. Hirsch, *Angew. Chem., Int. Ed.*, 2010, **49**, 3322–3325.
35 A. Catheline, C. Vallés, C. Drummond, L. Ortolani, V. Morandi, M. Marcaccio, M. Iurlo, F. Paolucci and A. Pénicaud, *Chem. Commun.*, 2011, **47**, 5470.
36 S. Pekker, J.-P. Salvetat, E. Jakab, J.-M. Bonard and L. Forró, *J. Phys. Chem. B*, 2001, **105**, 7938–7943.
37 M. Bockrath, J. Hone, A. Zettl, P. L. McEuen, A. G. Rinzler and R. E. Smalley, *Phys. Rev. B: Condens. Matter*, 2000, **61**, R10606–R10608.
38 Y. Gotoh, K. Tamada, N. Akuzawa, M. Fujishige, K. Takeuchi, M. Endo, R. Matsumoto, Y. Soneda and T. Takeichi, *J. Phys. Chem. Solids*, 2013, **74**, 1482–1486.
39 T. Enoki, S. Miyajima, M. Sano and H. Inokuchi, *J. Mater. Res.*, 1990, **5**, 435–466.
40 T. Enoki, M. Sano and H. Inokuchi, *Phys. Rev. B: Condens. Matter*, 1985, **32**, 2497–2505.
41 D. E. Bergbreiter and J. M. Killough, *J. Chem. Soc., Chem. Commun.*, 1976, 913b.
42 G. Bepete, E. Anglaret, L. Ortolani, V. Morandi, K. Huang, A. Pénicaud and C. Drummond, *Nat. Chem.*, 2016, DOI: 10.1038/nchem.2699.
43 P. Vecera, J. Holzwarth, K. F. Edelthalhammer, U. Mundloch, H. Peterlik, F. Hauke and A. Hirsch, *Nat. Commun.*, 2016, **7**, 1–7.
44 J. E. Swartz and T. T. Stenzel, *J. Am. Chem. Soc.*, 1984, **106**, 2520–2524.
45 Y. Wei, X. Dang and S. Hu, *Russ. J. Electrochem.*, 2004, **40**, 400–404.
46 G. Boschloo and A. Hagfeldt, *Acc. Chem. Res.*, 2009, **42**, 1819–1826.
47 T. Kaiho, *Iodine Chemistry and Applications*, John Wiley & Sons, 2014.
48 M. D. Diener, J. W. Raebiger, R. D. Bolskar and J. M. Alford, *US* 7794682B1, 2010.
49 A. Hirsch and M. Brettreich, *Fullerenes: Chemistry and Reactions*, John Wiley & Sons, 2006.

50 C. A. Reed and R. D. Bolskar, *Chem. Rev.*, 2000, **100**, 1075–1120.
51 M. Gomberg, *J. Am. Chem. Soc.*, 1900, **22**, 757–771.
52 R. A. Moss, M. S. Platz and M. J. Jones, *Reactive Intermediate Chemistry*, John Wiley & Sons, 2004.
53 R. Breslow, W. Bahary and W. Reinmuth, *J. Am. Chem. Soc.*, 1961, **83**, 1763–1764.
54 H. Volz and W. Lotsch, *Tetrahedron Lett.*, 1969, **10**, 2275–2278.
55 H. E. Zieger, I. Angres and L. Maresca, *J. Am. Chem. Soc.*, 1973, **95**, 8201–8203.
56 C. A. Howard, M. P. M. Dean and F. Withers, *Phys. Rev. B: Condens. Matter*, 2011, **84**, 241404.
57 D. Yang, A. Velamakanni, G. Bozoklu, S. Park, M. Stoller, R. D. Piner, S. Stankovich, I. Jung, D. A. Field, C. A. Ventrice and R. S. Ruoff, *Carbon*, 2009, **47**, 145–152.
58 C. Buono, P. R. Davies, R. J. Davies, T. Jones, J. Kulhavý, R. Lewis, D. J. Morgan, N. Robinson and D. J. Willock, *Faraday Discuss.*, 2014, **173**, 257–272.
59 K. A. Wepasnick, B. A. Smith, K. E. Schrote, H. K. Wilson, S. R. Diegelmann and D. H. Fairbrother, *Carbon*, 2011, **49**, 24–36.
60 V. V. Gobre and A. Tkatchenko, *Nat. Commun.*, 2013, **4**, 2341.
61 N. Karousis, A. S. D. Sandanayaka, T. Hasobe, S. P. Economopoulos, E. Sarantopoulou and N. Tagmatarchis, *J. Mater. Chem.*, 2011, **21**, 109–117.
62 C. Zhang, M. Chen, X. Xu, L. Zhang, L. Zhang, F. Xia, X. Li, Y. Liu, W. Hu and J. Gao, *Nanotechnology*, 2014, **25**, 135707.
63 F. Cardarelli, *Materials Handbook: A Concise Desktop Reference*, Springer Science & Business Media, 2nd edn, 2008.
64 T. Yoshida, K. Yamasaki and S. Sawada, *Bull. Chem. Soc. Jpn.*, 1978, **51**, 1561–1562.
65 A. C. Ferrari and J. Robertson, *Phys. Rev. B: Condens. Matter*, 2000, **61**, 14095–14107.
66 A. C. Ferrari, *Solid State Commun.*, 2007, **143**, 47–57.
67 C. Jiang, Z. Peng, C. de los Reyes, C. C. Young, D. E. Tsentalovich, V. Jamali, P. M. Ajayan, J. M. Tour, M. Pasquali and A. A. Martí, *Chem. Commun.*, 2017, **53**, 1498–1501.
68 P. L. Cullen, K. M. Cox, M. K. Bin Subhan, L. Picco, O. D. Payton, D. J. Buckley, T. S. Miller, S. A. Hodge, N. T. Skipper, V. Tileli and C. A. Howard, *Nat. Chem.*, 2016, DOI: 10.1038/nchem.2650.